

基于光纤端面双光子聚合微柱的丙酮气体传感器

刘丹^{1,2}, 赵聪^{1,2}, 纪朋^{1,2}, 蔡智濠^{1,2}, 李博哲^{1,2}, 邹梦强^{1,2}, 廖常锐^{1,2*}¹深圳大学物理与光电工程学院教育部/广东省光电子器件与系统重点实验室, 广东 深圳 518060;²深圳大学广东省光纤传感技术粤港联合研究中心深圳市物联网光子器件与传感系统重点实验室, 广东 深圳 518060

摘要 随着社会经济水平的不断提高, 糖尿病患者数量和比例正在迅速增加。目前糖尿病人的血糖浓度监测都是通过血糖仪实现, 这种有创的方法不仅繁琐, 还会给病人造成负担和痛苦, 不适合作为糖尿病患者血糖浓度的长期监测手段。呼吸气体中的丙酮浓度可以反映人体的血糖浓度, 因此, 可以用无创的方式, 通过测量呼吸气体中丙酮的浓度来达到对糖尿病患者血糖浓度监测的目的。通过飞秒激光诱导的双光子聚合技术, 在单模光纤端面制备了聚合物微柱, 设计了一种用于丙酮气体浓度检测的新型光纤传感器。当构成微柱的聚合物材料吸收丙酮气体后, 由微柱结构与光纤端面构成的法布里-珀罗干涉仪的反射光谱会发生相应的漂移。传感器对丙酮气体浓度的检测范围为 $1 \times 10^{-9} \sim 1 \times 10^{-3}$, 检测下限达到 1×10^{-9} , 传感器具备对呼吸气体中低浓度丙酮气体检测的能力。该传感器具有高灵敏度、高集成度、简单易用等特点, 有望通过无创的呼吸检测方式, 成为糖尿病人血糖浓度检测的新手段。

关键词 传感器; 双光子聚合; 法布里-珀罗干涉仪; 光纤传感; 丙酮; 糖尿病

中图分类号 TN249

文献标志码 A

DOI: 10.3788/CJL202249.1210002

1 引言

糖尿病是身体不能分泌或者不能正常分泌胰岛素而引起的一种非传染性的人体代谢疾病。近年来, 糖尿病患者越来越多^[1]。为了改善生活质量和节省医疗资源, 有必要进一步优化糖尿病的检测手段, 持续提升糖尿病的治疗水平^[2-3]。呼吸是人体和外界进行气体交换的过程, 是人体最为重要的代谢活动之一。呼出气体蕴含大量与身体健康状况相关的信息。正常人呼出的气体中含有数百种挥发性有机化合物(VOC), 其成分和浓度反映了人体的新陈代谢情况。丙酮被认为是 I 型糖尿病的生物标志物, 在正常人的呼吸气体中, 其浓度处于 0.39×10^{-6} 到 0.85×10^{-6} 范围内^[4]。而在糖尿病患者的呼出气体中, 丙酮的含量相较于正常人显著偏高^[5], 因此, 可以通过检测呼吸气体中的丙酮浓度来监测糖尿病患者的病情^[6-7]。

目前广泛使用的丙酮气体检测手段主要有三种, 分别是气相色谱法、质谱法、激光光谱法^[8]。这三种方法虽然精度很高, 但是因为设备昂贵复杂, 无法作为糖尿病患者日常呼吸检测的方法。过去几十年, 随着半导体气敏传感器制备技术的发展, 研究人员开始将电化学传感器应用于丙酮气体检测^[9-11]。化学传感器的优点是体积小、价格低廉、易封装、灵敏度高、简单易操作等, 但有抗环境干扰能力弱、选择性较差、恢复时间长等缺点^[12]。

近年来, 飞秒激光诱导的双光子聚合技术作为一种超高精度的 3D 打印技术, 凭借其高制造精度和高灵活性的特点, 已经在光子学、微机械、微流控和生物医学等领域中得到了广泛的应用。将双光子聚合技术与光纤传感技术结合, 开发出的新型光纤集成微纳功能器件具有高精度和高灵活性等特点^[13-15], 为气体传感提供了一条新途径。深圳大学 Xiong 等^[16]利用飞秒激光诱导双光子聚合技术, 在

收稿日期: 2022-01-11; 修回日期: 2022-02-11; 录用日期: 2022-03-09

基金项目: 国家自然科学基金(62122057, 62075136)、广东省国际科技合作项目(2020A0505100066)、深圳市优秀科技青年人才培养项目(RCYX20200714114524139)

通信作者: *cliao@szu.edu.cn

光纤端面打印出聚合物微悬臂梁,并用磁控溅射技术在其表面覆盖钼薄膜,用于氢气的特异性检测,当氢气浓度(体积分数)从 0% 上升到 4.5% 时,传感器的灵敏度达到了 -0.02 nm ,为氢气检测提供了一种快速高灵敏的光学解决方案。

本文提出了一种基于光纤端面聚合物微柱结构的丙酮气体传感方案。在光纤端面聚合的光刻胶微柱吸收丙酮气体分子后,聚合物-丙酮分子的混合材料折射率发生变化,进而使光刻胶微柱与光纤端面构成的法布里-珀罗干涉仪(FPI)的反射干涉光谱发生漂移,光谱的漂移量能够反映被测丙酮气体的浓度。本文提出的传感器对丙酮气体浓度响应的检测范围达到 1×10^{-9} 至 1×10^{-3} ,检测下限达到 $1 \times$

10^{-9} ,能够满足对呼吸气体中低浓度丙酮气体的检测需求。

2 基本原理

图 1 是基于单模光纤(SMF)端面聚合物微柱结构的丙酮气体传感原理示意图。光刻胶微柱的上表面与光纤端面构成 FPI,氮气环境中的初始反射光谱如图 1 光谱图中实色曲线所示。当丙酮气体分子被微柱的聚合物材料吸收后,聚合物材料和丙酮气体混合物的折射率增大^[17],导致反射光谱发生蓝移,如图 1 光谱图中虚线所示。因此,FPI 反射光谱的漂移量可反映被测丙酮气体的浓度。以下是对丙酮气体传感机理的详细说明。

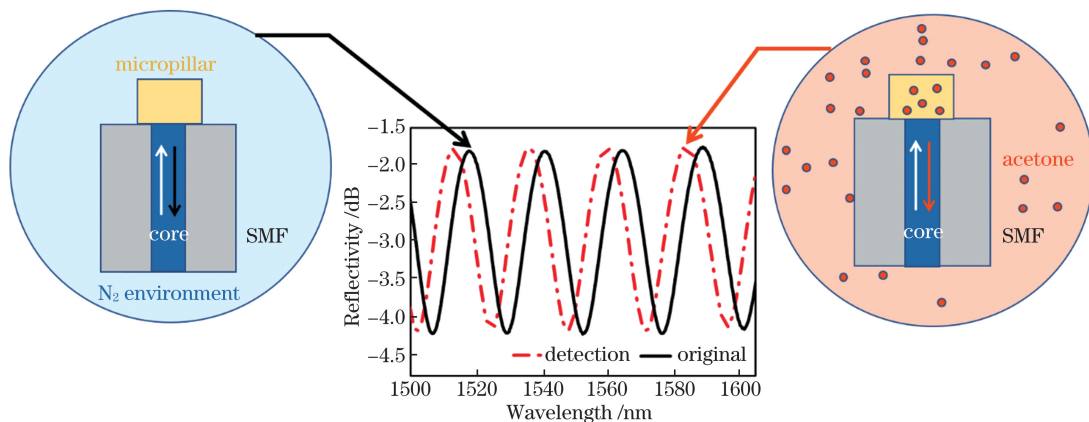


图 1 基于光纤端面微柱结构的丙酮气体传感原理图

Fig. 1 Principle diagram of acetone gas sensing based on fiber-tip micropillar

由光纤端面和微柱上表面构成的 FPI 的反射光谱漂移量 $\Delta\lambda$ 满足^[18]

$$\frac{\Delta\lambda}{\lambda} = \frac{\Delta L}{L} + \frac{\Delta n}{n}, \quad (1)$$

式中: λ 是反射光谱的波长; L 是微柱法布里-珀罗腔腔长; n 是聚合物材料的折射率; ΔL 是微柱法布里-珀罗腔腔长的改变量; Δn 是微柱聚合物材料折射率的改变量。

从式(1)中可以看出,吸收丙酮气体分子后,FPI 的腔长变化 ΔL 和 FPI 的介质(即光刻胶材料)折射率变化 Δn 都将导致反射光谱的漂移。有文献研究表明,对于玻璃状聚合物(glassy polymers),吸收 VOC 分子后聚合物的膨胀效应不显著,对 FPI 反射光谱漂移的贡献非常小,即可以忽略腔长变化($\Delta L/L$)的影响^[19-21]。由于本研究采用的光刻胶性质接近玻璃状聚合物的特性,因此,FPI 反射光谱的漂移主要是聚合物微柱吸收丙酮气体后折射率变化引起的。

3 器件制备

基于飞秒激光双光子聚合技术的光纤端面聚合物微柱制备过程如图 2 所示。首先,将包层直径为 $125 \mu\text{m}$ 、纤芯直径约为 $8 \mu\text{m}$ 的单模光纤切平后放置在方形玻片上,然后将切平的端面浸没于负性光刻胶中并盖上盖玻片,如图 2(a)所示。实验采用的光刻胶材料的主要成分是 2.5% (摩尔分数)的 IGR-369、40% (摩尔分数)的 SR444 单体、25% (摩尔分数)的 454 单体、30% (摩尔分数)的 SR368 单体、2% (摩尔分数)的四乙基秋兰姆二硫化物(TED)、0.5% (摩尔分数)的 4-羟基茴香醚(MEHQ)。其中,IGR 作为光引发剂激发双光子吸收,SR444 单体用于保证光刻胶溶液的黏稠度,SR454 用于提高聚合物的机械强度,SR368 单体用于提高光刻胶的光敏性和机械强度。

随后将样品固定在精密三维气浮位移平台上,利用飞秒激光进行聚合,如图 2(b)所示。聚合过程

所使用的飞秒激光器输出的脉冲宽度为 290 fs, 中心波长为 1026 nm, 脉冲重复频率为 200 kHz^[16]。在保证聚合质量的前提下, 选用 50 倍物镜进行聚合

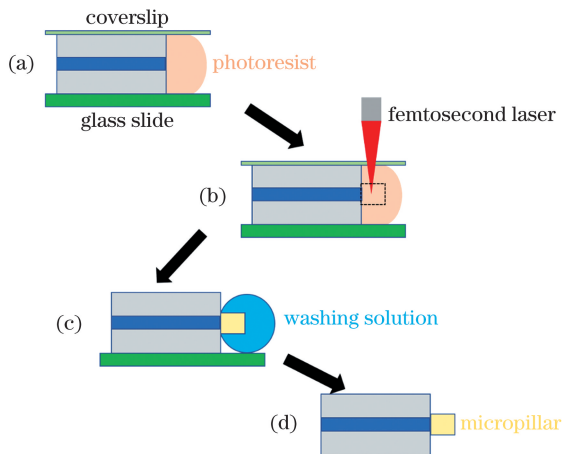


图 2 器件制作流程图。(a)将光刻胶溶液滴在单模光纤端面并盖上盖玻片;(b)利用双光子聚合在光纤端面聚合微柱结构;(c)拆除光纤顶部的盖玻片,用异丙醇和丙酮的混合溶液清除未固化的光刻胶;(d)微柱聚合在光纤端面

Fig. 2 Flow chart of device fabrication. (a) Photoresist solution dropped on end face of single-mode fiber, covered with coverslip; (b) two-photon polymerization for micropillar structure on end face of fiber; (c) coverslip on top of optical fiber removed and uncured photoresist washed away with mixed solution of isopropyl alcohol and acetone; (d) micropillar fabricated on end face of optical fiber

以获得更高的制备效率, 采用的激光脉冲能量约为 10 nJ, 位移平台的扫描速度为 300 $\mu\text{m/s}$, 线间距为 500 nm, 层间距为 500 nm。激光聚合过程结束后, 移除胶带及盖玻片, 将样品在丙酮和异丙醇的混合洗胶溶液(体积比为 1:4)中浸泡约 1 min 进行显影, 如图 2(c)所示。提高混合洗胶溶液中丙酮的浓度可加快显影的速度, 但残留的显影液会在挥发时引入较大的表面张力, 从而破坏结构。洗胶溶液中丙酮浓度过低将增加显影时间, 从而降低光纤端面与微柱之间的黏附牢固性。显影后微柱结构牢固粘连于光纤端面上, 如图 2(d)所示。

4 实验结果与讨论

为了评估双光子聚合光纤端面微柱的加工质量, 我们制备了设计高度为 20 μm 的微柱并利用扫描电子显微镜(SEM)对其形貌进行表征。如图 3 所示, 光纤端面聚合物微柱完全覆盖纤芯, 形貌完整。设计高度为 20 μm 的微柱在聚合完毕后实测高度约为 19.6 μm , 其误差值约为 2%。产生误差的原因主要有: 1) 为了保证结构能够完好粘连于光纤端面上, 加工不是从光纤端面开始的, 这将导致实际样品尺寸相比设计值略微缩小; 2) 聚合过程中激光能量的选择以及显影时长的偏差也会影响最终样品的尺寸。

采用宽带光源和光谱分析仪测量光纤端面聚合微柱传感器的反射光谱, 其自由光谱范围(FSR, F_s)^[22]为

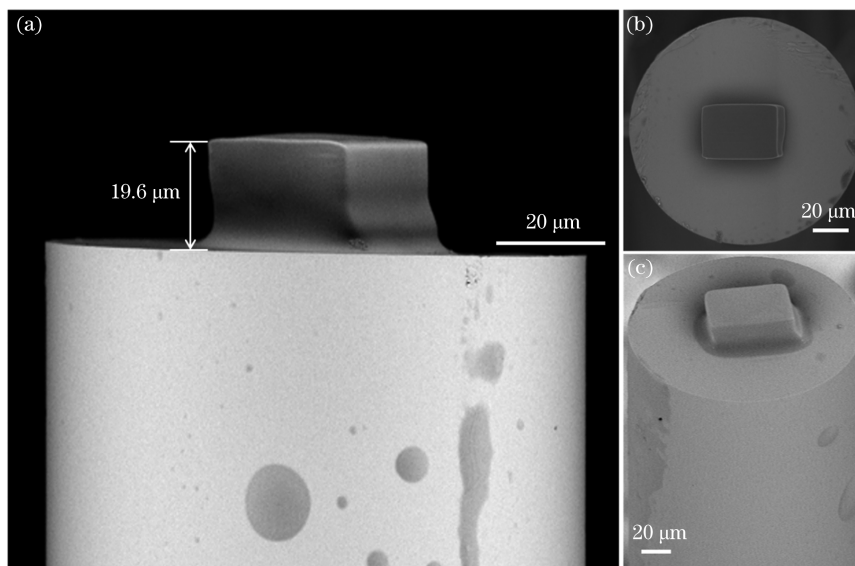


图 3 利用双光子聚合技术制备的光纤端面聚合物微柱的 SEM 图。(a)正视图;(b)俯视图;(c)侧视图

Fig. 3 SEM micrograph of polymerized micropillar fabricated on end face of optical fiber by two-photon polymerization.

(a) Front view; (b) vertical view; (c) side view

$$F_s = \frac{\lambda_1^2}{2nL}, \quad (2)$$

式中: λ_1 为干涉光谱波谷对应的波长。

图 4 展示了微柱为不同高度 (H_1, H_2, H_3) 时

的反射光谱及其在 1550 nm 处的 FSR 值。高度设计值为 20, 30, 40 μm 的器件对应的 FSR 值分别为 34.28, 24.56, 19.60 nm, 其变化趋势符合式 (2) 中描述的 F_s 与 L 的反比关系。

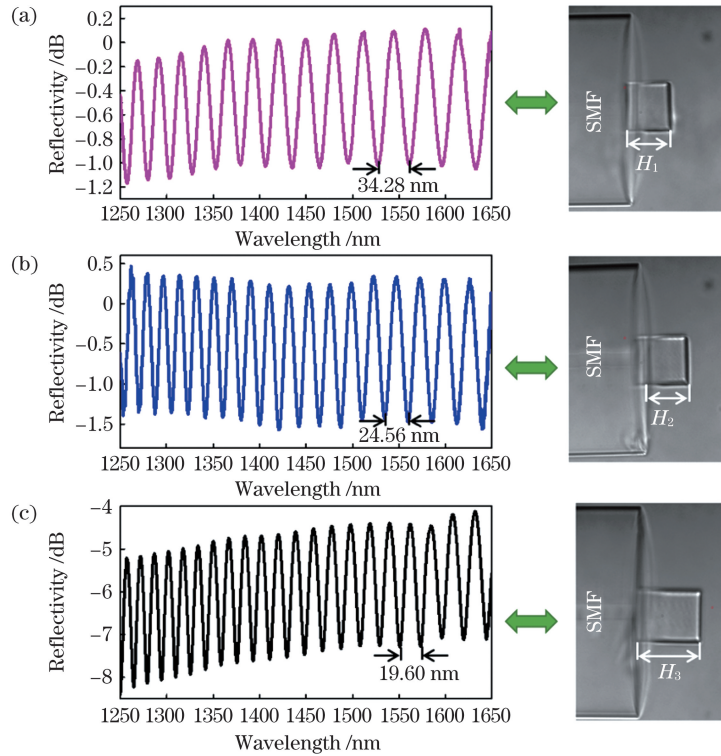


图 4 不同设计高度光纤端面聚合物微柱的反射光谱图。(a) $H_1 = 20 \mu\text{m}$; (b) $H_2 = 30 \mu\text{m}$; (c) $H_3 = 40 \mu\text{m}$

Fig. 4 Reflection spectra of polymerized micropillars on end face of optical fiber with different design heights.

(a) $H_1 = 20 \mu\text{m}$; (b) $H_2 = 30 \mu\text{m}$; (c) $H_3 = 40 \mu\text{m}$

本文对传感器在不同浓度丙酮气体中的光谱响应进行了测量。实验采用由惰性材料特氟龙制成的气体采样袋, 由于它对 VOC 分子的吸附性极低, 因此可以避免气袋材料对丙酮气体的吸附造成的误差。对于高浓度 (体积分数为 10^{-6} 级) 的丙酮气体^[23], 有

$$V_x = \frac{V \times C \times M}{22.4 \times d \times P} \times 10^{-9} \times \frac{273 + T_R}{273 + T_B}, \quad (3)$$

式中: V_x 为液体丙酮注入量的体积 (单位为 mL); V 为气袋的容积 (单位为 mL); C 为丙酮气体的浓度 (10^{-6} 量级); M 为丙酮的体积质量 (单位为 g/mL); d 为液体丙酮的密度 (g/cm^3); P 为液体纯度; T_R 为室温 (单位为 $^\circ\text{C}$); T_B 为配气袋内温度 (单位为 $^\circ\text{C}$)。

配气前, 在容积为 3 L 的气袋中先充入一定量的干燥氮气, 再根据式 (3), 将一定体积的液体丙酮用微量注射针注入气袋中, 然后再次向气袋中充入氮气将气体体积补足至 3 L, 最后, 将气袋置于 $65 \text{ }^\circ\text{C}$ 的烘箱中使丙酮液体完全挥发并均匀分布于

气袋中。待气袋的温度降至室温时, 将传感器置于气袋中进行检测。对于低浓度 (10^{-9} 量级) 的丙酮气体, 则采用逐级稀释的方法, 即按比例在氮气中加入高浓度的丙酮气体稀释得到。

本文以一个数量级为步进, 测试了微柱高度为 $30 \mu\text{m}$ 的传感器在体积分数为 $1 \times 10^{-9} \sim 1 \times 10^{-3}$ 的丙酮气体中的响应。如图 5(a) 所示, 在 1550 nm 附近, 随着丙酮气体的浓度升高, FPI 的反射光谱向短波方向移动, 在 $1 \times 10^{-9} \sim 1 \times 10^{-3}$ 的浓度 (体积分数, 全文同) 范围内, 反射光谱共漂移约 5 nm。以上现象可由聚合物微柱吸收丙酮气体分子后, 材料折射率增大来解释。图 5(b) 展示了各个丙酮浓度下反射光谱波谷波长的位置图。可以看出, 波谷波长随环境中丙酮浓度的增加而减小。当丙酮气体浓度小于 1×10^{-7} 时, 波谷波长的下降趋势变缓。这是由于当被测丙酮气体浓度很低时, 聚合物材料吸收到的丙酮分子非常有限, 此时丙酮气体浓度已经接近传感器的检测下限。因此, 我们将传感器的检测下限定为 1×10^{-9} , 检测范围为 $1 \times 10^{-9} \sim 1 \times 10^{-3}$ 。

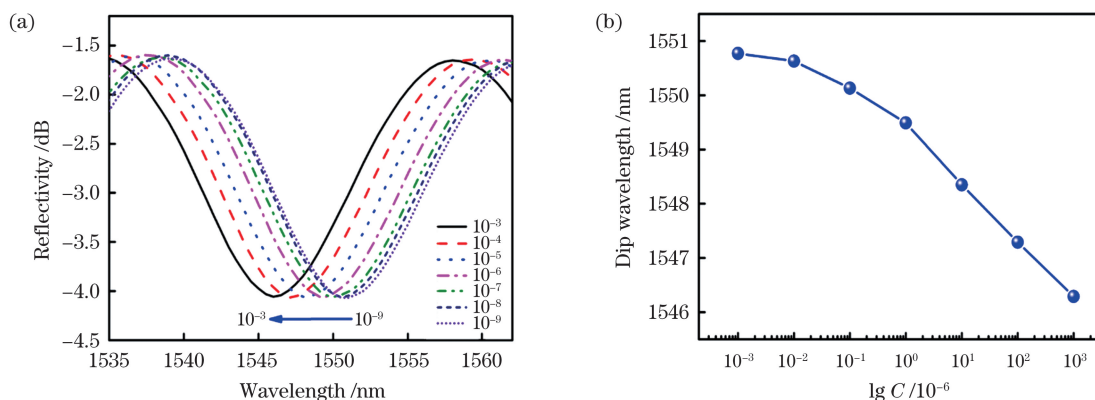


图 5 丙酮气体灵敏度测试。(a)不同丙酮浓度下的反射光谱;(b)波谷波长与丙酮浓度的关系

Fig. 5 Acetone gas sensitivity test. (a) Reflection spectra at different acetone concentrations ; (b) relationship between dip wavelength and acetone concentration

图 6 是传感器对浓度为 $1 \times 10^{-9} \sim 1 \times 10^{-3}$ 的丙酮气体响应的重复性测试结果。在三次测试中,保持一个数量级的步进,丙酮气体浓度由最低的 1×10^{-9} 上升至最高的 1×10^{-3} ,再下降回到 1×10^{-9} 。在每个气体浓度下,传感器在相应的气袋中静置 2 min 以上,待光谱稳定后记录数据。当被测丙酮气体浓度由 1×10^{-9} 上升至 1×10^{-3} 时,传感器反射光谱在 1550 nm 波长附近的蓝移量分别为 4.46, 4.51, 4.48 nm;在浓度由 1×10^{-3} 下降至 1×10^{-9} 时,1550 nm 波长处反射光谱的红移量分别为 4.42, 4.50, 4.53 nm。在该测试中,同一气体浓度对应的波长漂移量标准差均小于 5%。引起误差的主要原因是器件在测试过程中受到的轻微扰动以及丙酮气体配置的误差等。因此,传感器对浓度为 $1 \times 10^{-9} \sim 1 \times 10^{-3}$ 的丙酮气体的响应具有良好的重复性,有望成为稳定的日常呼吸气体丙酮的监测手段。

为了研究传感器的温度响应,将其置于控温精度为 $0.1 \text{ }^\circ\text{C}$ 的恒温炉中,并在常压下以 $5 \text{ }^\circ\text{C}$ 为步进,将温度从 $25 \text{ }^\circ\text{C}$ 提高到 $55 \text{ }^\circ\text{C}$ 。传感器在每个温度下

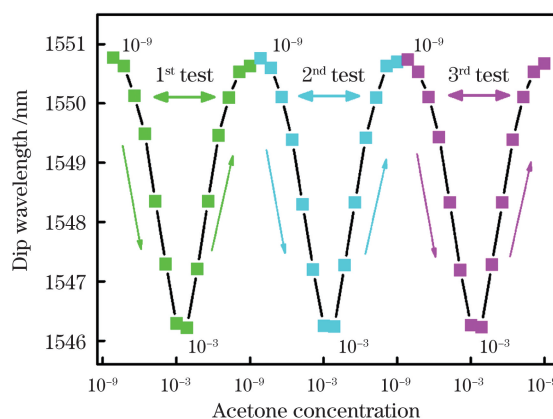


图 6 丙酮浓度在 $1 \times 10^{-9} \sim 1 \times 10^{-3}$ 之间先下降再上升循环三次时,聚合物微柱传感器的干涉光谱波谷波长的变化

Fig. 6 Variation of dip wavelength in interference spectrum of polymerized micropillar when acetone concentration first decreases and then increases for three times in range of 1×10^{-9} to 1×10^{-3}

静置至少 15 min 后,记录其反射光谱的漂移结果。如图 7 所示,传感器的反射光谱随温度的升高而发

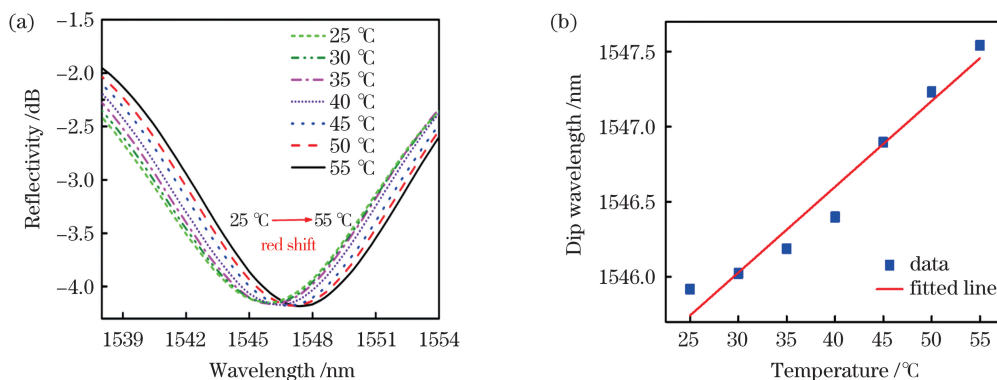


图 7 传感器的温度响应。(a)聚合物微柱传感器在不同温度下的干涉光谱响应;(b)干涉光谱波谷波长与环境温度的关系
Fig. 7 Temperature response of sensor; (a) Interference spectral response of polymerized micropillar sensor at different temperatures; (b) relationship between dip wavelength in interference spectrum and ambient temperature

生红移。这是由于当环境温度升高时,聚合物微柱受热膨胀,FPI腔长增大,进而干涉光谱发生红移。在25~55℃范围内,传感器的波谷波长漂移与温度的变化呈线性关系(相关系数 $R^2=0.95045$)灵敏度为60 pm/℃。在通常的呼吸检测中,气体温度的变化范围一般为25~35℃^[24],根据温度拟合曲线计算得到,对应的干涉波长漂移量为0.6 nm。与丙酮气体浓度在 $1\times 10^{-9}\sim 1\times 10^{-3}$ 范围内的反射光谱漂移量5 nm相比,温度变化会在丙酮气体浓度的检测结果中引入较大串扰。因此,在后续的呼吸检测中,需要严格控制被测呼吸气体的温度,将其稳定在室温左右进行测量,以保证丙酮浓度检测的准确性。

5 结 论

基于双光子聚合技术在光纤端面制备了聚合微柱,构造了法布里-珀罗干涉仪进行丙酮气体传感检测的方法。该传感器对丙酮气体的检测范围为 $1\times 10^{-9}\sim 1\times 10^{-3}$,检测下限为 1×10^{-9} ,且具有较好的重复性。研究结果为呼吸气体中丙酮的检测提供了一种高灵敏度、高集成度、简单易用的新方法。若进一步引入对丙酮具有特异性吸收能力的新型光刻胶材料进行传感器制备,所提出的传感器将有望走向实际临床应用,该无创的呼吸检测方法将成为糖尿病人血糖浓度检测的新手段。

参 考 文 献

- [1] Wild S, Roglic G, Green A, et al. Global prevalence of diabetes: estimates for the year 2000 and projections for 2030 [J]. *Diabetes Care*, 2004, 27(5): 1047-1053.
- [2] Ramachandran A, Ma R C W, Snehalatha C. Diabetes in Asia[J]. *The Lancet*, 2010, 375(9712): 408-418.
- [3] Zimmet P Z, Magliano D J, Herman W H, et al. Diabetes: a 21st century challenge [J]. *The Lancet Diabetes & Endocrinology*, 2014, 2(1): 56-64.
- [4] Solga S F. Breath volatile organic compounds for the gut-fatty liver axis: promise, peril, and path forward [J]. *World Journal of Gastroenterology*, 2014, 20(27): 9017-9025.
- [5] Zhou M G, Liu Y, Li W W, et al. Investigation and identification of breath acetone as a potential biomarker for type 2 diabetes diagnosis [J]. *Chinese Science Bulletin*, 2014, 59(17): 1992-1998.
- [6] Shokrehodaie M, Quinones S. Review of non-invasive glucose sensing techniques: optical, electrical and breath acetone [J]. *Sensors*, 2020, 20(5): 1251.
- [7] 孙利群, 邹明丽, 王旋. 可调谐半导体激光吸收光谱法在呼吸诊断中的应用 [J]. *中国激光*, 2021, 48(15): 1511001.
Sun L Q, Zou M L, Wang X. Application of tunable diode laser absorption spectroscopy in breath diagnosis [J]. *Chinese Journal of Lasers*, 2021, 48(15): 1511001.
- [8] Anderson J C. Measuring breath acetone for monitoring fat loss: review [J]. *Obesity*, 2015, 23(12): 2327-2334.
- [9] Wang C J, Sahay P. Breath analysis using laser spectroscopic techniques: breath biomarkers, spectral fingerprints, and detection limits [J]. *Sensors*, 2009, 9(10): 8230-8262.
- [10] Wang Z N, Wang C J. Is breath acetone a biomarker of diabetes? A historical review on breath acetone measurements [J]. *Journal of Breath Research*, 2013, 7(3): 037109.
- [11] 孙美秀, 赵晓萌, 王振南, 等. 面向医学研究的便携式CRDS呼吸丙酮分析仪 [J]. *中国激光医学杂志*, 2016, 25(5): 255.
Sun M X, Zhao X M, Wang Z N, et al. Portable CRDS acetone analyzer for medical research [J]. *Chinese Journal of Laser Medicine & Surgery*, 2016, 25(5): 255.
- [12] Storer M, Dummer J, Lunt H, et al. Measurement of breath acetone concentrations by selected ion flow tube mass spectrometry in type 2 diabetes [J]. *Journal of Breath Research*, 2011, 5(4): 046011.
- [13] Zhang Y F, Lin C P, Liao C R, et al. Femtosecond laser-inscribed fiber interface Mach-Zehnder interferometer for temperature-insensitive refractive index measurement [J]. *Optics Letters*, 2018, 43(18): 4421-4424.
- [14] Zhang Y F, Liao C R, Lin C P, et al. Surface plasmon resonance refractive index sensor based on fiber-interface waveguide inscribed by femtosecond laser [J]. *Optics Letters*, 2019, 44(10): 2434-2437.
- [15] 何飞, 程亚. 飞秒激光微加工: 激光精密加工领域的新前沿 [J]. *中国激光*, 2007, 34(5): 595-622.
He F, Cheng Y. Femtosecond laser micromachining: frontier in laser precision micromachining [J]. *Chinese Journal of Lasers*, 2007, 34(5): 595-622.
- [16] Xiong C, Zhou J T, Liao C R, et al. Fiber-tip polymer microcantilever for fast and highly sensitive hydrogen measurement [J]. *ACS Applied Materials & Interfaces*, 2020, 12(29): 33163-33172.
- [17] Albert K J, Lewis N S, Schauer C L, et al. Cross-reactive chemical sensor arrays [J]. *Chemical Reviews*, 2000, 100(7): 2595-2626.

- [18] Lemieux-Leduc C, Guertin R, Bianki M A, et al. All-polymer whispering gallery mode resonators for gas sensing[J]. *Optics Express*, 2021, 29(6): 8685-8697.
- [19] Ji P, Zhu M, Liao C R, et al. In-fiber polymer microdisk resonator and its sensing applications of temperature and humidity [J]. *ACS Applied Materials & Interfaces*, 2021, 13(40): 48119-48126.
- [20] St-Gelais R, Mackey G, Saunders J, et al. Gas sensing using polymer-functionalized deformable Fabry-Perot interferometers [J]. *Sensors and Actuators B: Chemical*, 2013, 182: 45-52.
- [21] Abgrall P, Conedera V, Camon H, et al. SU-8 as a structural material for labs-on-chips and microelectromechanical systems[J]. *Electrophoresis*, 2007, 28(24): 4539-4551.
- [22] Luo J X, Liu S, Chen P J, et al. Fiber optic hydrogen sensor based on a Fabry-Perot interferometer with a fiber Bragg grating and a nanofilm[J]. *Lab on a Chip*, 2021, 21(9): 1752-1758.
- [23] 史黎薇, 任改英, 井海宁. 低浓度挥发性有机物混合标准气体的配制[J]. *中国卫生工程学*, 2005, 4(6): 353-355.
- Shi L W, Ren G Y, Jing H N. Preparation of mixed standard gases of VOCs in low concentration [J]. *Chinese Journal of Public Health Engineering*, 2005, 4(6): 353-355.
- [24] Amann A, Poupart G, Telser S, et al. Applications of breath gas analysis in medicine[J]. *International Journal of Mass Spectrometry*, 2004, 239(2/3): 227-233.

Acetone Gas Sensor Based on Two-Photon Polymerized Micropillar on End Face of Fiber

Liu Dan^{1,2}, Zhao Cong^{1,2}, Ji Peng^{1,2}, Cai Zhihao^{1,2}, Li Bozhe^{1,2}, Zou Mengqiang^{1,2}, Liao Changrui^{1,2*}

¹ Key Laboratory of Optoelectronic Devices and Systems of Ministry of Education/Guangdong Province, College of Physics and Optoelectronic Engineering, Shenzhen University, Shenzhen 518060, Guangdong, China; ² Shenzhen Key Laboratory of Photonic Devices and Sensing Systems for Internet of Things, Guangdong and Hong Kong Joint Research Centre for Optical Fibre Sensors, Shenzhen University, Shenzhen 518060, Guangdong, China

Abstract

Objective Diabetes is a kind of non-infectious human metabolic disease caused by the inability to secrete insulin or secrete insulin normally. In recent years, the prevalence of diabetes has become much higher than before. In order to improve the life of patients and save the medical resources, it is necessary to further optimize the detection methods of diabetes. Human breath contains numerous information related to health. The breath of healthy people contains hundreds of volatile organic compounds (VOCs), whose composition and concentration can reflect the metabolism of a human body. The concentration of glucose in the blood of diabetic patients can be reflected by detecting the acetone concentration in breath. At present, the acetone detection methods mainly include gas chromatography, mass spectrometry, and laser spectroscopy. The required equipment is usually expensive and complex, which limits their application as a daily breath detection method for diabetic patients. As an ultra-high-precision 3D printing technology, femtosecond-laser induced two-photon polymerization microfabrication has been widely used in the fields of photonics, micromachines, microfluidics, and biomedicine, due to its high manufacturing precision and flexibility. Combining the two-photon polymerization technology with fiber optical sensing, the developed integrated device has the characteristics of high precision and flexibility, which provides a new solution for gas sensing. In this study, we report an acetone gas sensing method based on the polymer micropillar structure fabricated on the end face of a fiber. The absorption of acetone molecules by the photoresist micropillars polymerized on the end face of the fiber leads to the change of refractive index of the polymer-acetone mixed material, and subsequently makes the reflection interference spectrum from the Fabry-Perot interferometer (composed of the photoresist micropillars and the fiber end face) shift.

Methods Two-photon polymerization is used to prepare the polymerized micropillars on the end face of a single-mode fiber. First, the single-mode fiber is cut flatly and placed on a glass slide. Then the cut end face is immersed in

the negative photoresist. The sample is fixed on a three-dimensional air-floating displacement platform and polymerized by a femtosecond laser. After the laser polymerization process is complete, the sample is developed in a mixed solution of acetone and isopropanol. After the development, the micropillar structure is firmly adhered on the end face of the optical fiber. The morphology of the fabricated device is characterized by scanning electron microscope. The reflection spectrum of the polymerized micropillar sensor is measured by a broadband light source and a spectrum analyzer. The reflection spectra and free spectral range (FSR) values of the micropillar at different heights are compared. The spectral response of the sensor to acetone concentration is also tested. The temperature response of the sensor and the influence of temperature change on acetone concentration in the daily breath detection are studied.

Results and Discussions In this study, the micropillar with a designed height of 20 μm is first characterized by scanning electron microscopy. The measured height of the micropillar is about 19.6 μm after polymerization (Fig. 3). The reflection spectra of micropillars with different heights and their FSR values at ~ 1550 nm are tested, showing that the heights of the micropillar devices are inversely proportional to their FSR values (Fig. 4). The spectral response of the sensor with a micropillar height of 30 μm to acetone concentration is measured. In the concentration range of 1×10^{-9} to 1×10^{-3} , the reflection spectrum shifts by 5 nm. The mechanism is that after the polymerized micropillar absorbs acetone gas molecules, the material refractive index increases (Fig. 5). The trough wavelength decreases with the increase of acetone concentration in the environment. When the acetone gas concentration is less than 1×10^{-7} , the decreasing trend of trough wavelength becomes slow. This is because when the acetone gas concentration is very low, the acetone molecules absorbed by the polymerized material are limited, which is close to the lower detection limit of the sensor. Thus, the detection limit of the sensor is determined to be 1×10^{-9} . The sensor is repeatedly tested using acetone gas with the concentration range of 1×10^{-9} to 1×10^{-3} . The blue shift of the sensor near 1550 nm in the reflection spectrum and the red shift of the sensor near 1550 nm are very similar, and both are with a close standard deviation of wavelength shift (less than 5%) (Fig. 6). The temperature response of the sensor from 25 $^{\circ}\text{C}$ to 55 $^{\circ}\text{C}$ is also studied. The reflection spectrum of the sensor shows a red shift with the increase of temperature. The reason is that with the increase of ambient temperature, the thermal expansion of polymerized micropillars leads to the increase of the FPI cavity length. During the detection, the temperature change introduces a large influence on the detection results of acetone concentration. It is necessary to strictly control the temperature of the gas to be tested and ensure the detection stability of acetone concentration (Fig. 7).

Conclusions In this paper, the method based on two-photon polymerization for polymerizing micropillars on end face of a fiber and constructing an FPI acetone gas sensor is proposed. The sensor has a detection range of 1×10^{-9} to 1×10^{-3} for acetone concentration and a detection limit of 1×10^{-9} . This work provides a new, high-sensitivity, high-integration, and simple-to-use method for the detection of acetone in breath. If a new type of photoresist material with specific absorption capacity for acetone is further applied in sensor preparation, the sensor proposed in this paper will be more useful in practical clinical applications. Through the non-invasive breath detection, it will become a new method for the detection of blood glucose concentration in diabetic patients.

Key words sensors; two-photon polymerization; Fabry-Perot interferometer; optical fiber sensing; acetone; diabetes